

Cite this: *J. Mater. Chem. A*, 2021, 9, 22262Received 1st August 2021
Accepted 20th September 2021

DOI: 10.1039/d1ta06498c

rsc.li/materials-a

Concomitant shape and palladium engineering of hollow conjugated microporous photocatalysts to boost visible light-induced hydrogen evolution†

Sang Hyun Ryu,^a Sang Moon Lee,^b Hae Jin Kim,^b Yoon-Joo Ko,^c Kyoung Chul Ko^{*d} and Seung Uk Son^{†*}

This work shows that the hydrogen evolution performance of conjugated microporous polymer (CMP)-based photocatalysts can be enhanced through their hollow shape engineering. Using a hollow microporous organic polymer (H-MOP) as a template, hollow Stille coupling-based CMP photocatalysts with Pd nanoparticles (H-MOP@SCMP-Pds) were prepared, showing enhanced hydrogen evolution rates up to $7100 \mu\text{mol h}^{-1} \text{g}^{-1}$ and apparent quantum yields up to 3.72% (@420 nm).

In 2014, our research group reported a conjugated microporous photocatalyst with the electronic push-pull structure for visible light-induced hydrogen evolution.¹ We introduced TiO_2 nanoparticles into the photocatalytic system for the facilitated charge separation. In addition, Pt was employed to reduce overpotentials in photo-induced redox catalysis. At that time, it was agreed that the use of the noble metal was a drawback.

Recently, there have been extensive and insightful studies of scientists on conjugated microporous polymer (CMP)-based photocatalysts for hydrogen evolution.² The band-gaps of CMP-based organic photocatalysts were delicately engineered through the scanning of aromatic building blocks.^{3,4} For the efficient absorption of visible light and photo-induced charge separation, push-pull chemical structures have been adopted for CMP-based photocatalytic systems.⁵⁻⁷ The effects of porous or nonporous features on photocatalytic performance were

studied.⁸⁻¹⁰ Recently, the photocatalytic composites of organic polymers with inorganic materials were engineered.^{11,12} The importance of residual or additional noble metals in the CMP-based photocatalysts has been reported for the enhanced hydrogen evolution.^{13,14} The recent progresses in the CMP-based photocatalysts have stimulated us to restudy CMP with noble metals as the photocatalytic systems for hydrogen evolution.

Our previous work¹ focused the chemical durability of organic photocatalysts in CMP/ TiO_2 -Pt. Because photo-induced electron transfer can result in the organic radical forms of photosensitizers,¹⁵ the irreversible coupling of the organic radical species can reduce the durability of photocatalytic systems. The networking of organic photocatalysts can suppress such irreversible coupling of radical intermediates and enhance the durability of photocatalytic systems, compared with molecular systems.¹⁶ In another hand, the photocatalytic activities of the CMP/ TiO_2 -Pt are considerable, displaying a hydrogen evolution rate (HER) of $1250 \mu\text{mol h}^{-1} \text{g}^{-1}$. The promising photocatalytic activity is attributable to the efficient visible light absorption by the donor-acceptor chemical structure, facile charge separation, and the reduced overpotentials by the Pt catalyst. Recently, Wang *et al.* reviewed the recent progresses in the CMP-based photocatalysts and their catalytic performance, showing a gradual improvement of HERs from $70 \mu\text{mol h}^{-1} \text{g}^{-1}$ to $3142 \mu\text{mol h}^{-1} \text{g}^{-1}$.²

Since the report of CMP/ TiO_2 -Pt, we have studied further engineering of CMPs based on Sonogashira coupling to improve the photocatalytic performance for hydrogen evolution. Unfortunately, we have been frustrated because the photocatalytic performance of the Sonogashira coupling-based CMP photocatalysts did not exceed those of the Knoevenagel condensation-based CMP/ TiO_2 -Pt of the previous paper.¹ Recently, we found that the self-supporting of Pd nanoparticles can be systematically controlled during the synthesis of Stille coupling-based CMP (SCMP) because the zerovalent Pd catalysts were used without additional bases.¹⁷ In addition, it has been well reported that the hollow morphology engineering of catalytic materials can enhance their performance.¹⁸⁻²² However,

^aDepartment of Chemistry, Sungkyunkwan University, Suwon 16419, Korea. E-mail: sson@skku.edu

^bKorea Basic Science Institute, Daejeon 34133, Korea

^cLaboratory of Nuclear Magnetic Resonance, National Center for Inter-University Research Facilities (NCIRF), Seoul National University, Seoul 08826, Korea

^dDepartment of Chemistry Education, Chonnam National University, Gwangju 61186, Korea. E-mail: kcco1982@jnu.ac.kr

† Electronic supplementary information (ESI) available: Experimental procedure, additional characterization data of H-MOP, H-MOP@SCMP-Pds, and SCMP-Pd, a computational simulation of SCMP and related files, characterization data of H-MOP@SCMP-Pd2 before and after catalytic reactions, AQY measurements, and HER performance comparison of the recent CMP-based photocatalysts. See DOI: 10.1039/d1ta06498c

unfortunately, our numerous trials for the shape-controlled synthesis of the hollow SCMP by the conventional silica template method^{23,24} were unsuccessful. Instead, we have found that the Sonogashira coupling-based hollow microporous organic polymer (H-MOP) can be utilized for the engineering of other CMPs.^{25,26} As the Sonogashira coupling-based MOP in this work is not fully conjugated, due to the existence of sp^3 carbons in the main chain skeletons, the term, MOP is used. Finally, we could develop hollow MOP@SCMP-based photocatalytic systems with Pd nanoparticles (H-MOP@SCMP-Pds) showing the HERs up to $7100 \mu\text{mol h}^{-1} \text{g}^{-1}$ under visible light irradiation. In this work, we report the engineering of SCMP on the hollow Sonogashira coupling-based MOP, the concomitant incorporation of Pd nanoparticles, and the enhanced photocatalytic performance for the hydrogen evolution.

Fig. 1 shows a synthetic scheme for H-MOP@SCMP-Pds. First, the H-MOP was prepared by the Sonogashira coupling of tetra(4-ethynylphenyl)methane²⁷ with 1,4-diiodobenzene in the presence of silica spheres with sizes of 200–240 nm and by successive silica etching through treatment of aqueous HF solution. Recently, Jiang *et al.* reported the development of CMP-based photocatalysts bearing dibenzothiophene sulfone moieties, displaying excellent performance in the visible light-induced hydrogen evolution.^{28–30} Considering the recent progresses,^{28–30} H-MOP@SCMP-Pds were prepared in the presence of the H-MOP template by the $(\text{PPh}_3)_4\text{Pd}$ -catalyzed Stille coupling of tris(4-trimethylstannylphenyl)amine with 3,7-dibromodibenzothiophene sulfone. With an optimized and fixed amount of building blocks and H-MOP, we increased the amount of

$(\text{PPh}_3)_4\text{Pd}$ catalysts from 8 μmol to 32 and 64 μmol . The resultant materials were denoted as H-MOP@SCMP-Pd1, H-MOP@SCMP-Pd2, and H-MOP@SCMP-Pd3, respectively. As a control material, nonhollow SCMP-Pd was prepared without H-MOP templates by the $(\text{PPh}_3)_4\text{Pd}$ (32 μmol)-catalyzed Stille coupling of tris(4-trimethylstannylphenyl)amine with 3,7-dibromodibenzothiophene sulfone.

The morphologies of H-MOP@SCMP-Pds were investigated by transmission electron microscopy (TEM) (Fig. 2). As shown in Fig. 2a, the H-MOP has a hollow structure with an average diameter of 223 nm and a shell thickness of 24 nm. As the amount of $(\text{PPh}_3)_4\text{Pd}$ catalyst increased, the diameters of H-MOP@SCMP-Pds increased gradually from 233 nm (H-MOP@SCMP-Pd1) to 245 (H-MOP@SCMP-Pd2) and 259 nm (H-MOP@SCMP-Pd3) with an increase of shell thicknesses from 30 nm to 35 and 43 nm, respectively, indicating the incorporation of ~ 5 , ~ 10 , and ~ 20 nm thick SCMP-Pds into H-MOP, respectively (Fig. 2b–d). Whilst the residual Pd species was not detectable in the TEM analysis of H-MOP and H-MOP@SCMP-Pd1, Pd nanoparticles appeared at H-MOP@SCMP-Pd2 and H-MOP@SCMP-Pd3 (Fig. 2a–d). The average sizes of Pd nanoparticles in H-MOP@SCMP-Pd2 and H-MOP@SCMP-Pd3 were measured to be 5.2 and 8.1 nm, respectively. In addition, as the amount of $(\text{PPh}_3)_4\text{Pd}$ catalyst increased, the number of Pd nanoparticles in H-MOP@SCMP-Pd2 and H-MOP@SCMP-Pd3 increased. The nonhollow SCMP-Pd had irregular morphologies with diameters of 100–250 nm and 2.0–4.5 nm-sized Pd particles (Fig. 2e).

The chemical composition of H-MOP@SCMP-Pd-2 was further investigated by energy dispersive X-ray spectroscopy (EDS). The EDS-based elemental mapping study of H-MOP@SCMP-Pd2 revealed the existence of Pd and the homogeneous distribution of N and S over hollow materials, originating from triphenylamine and dibenzothiophene sulfone moieties in the building blocks and supporting the successful incorporation of SCMP-Pd into the H-MOP template (Fig. 2f).

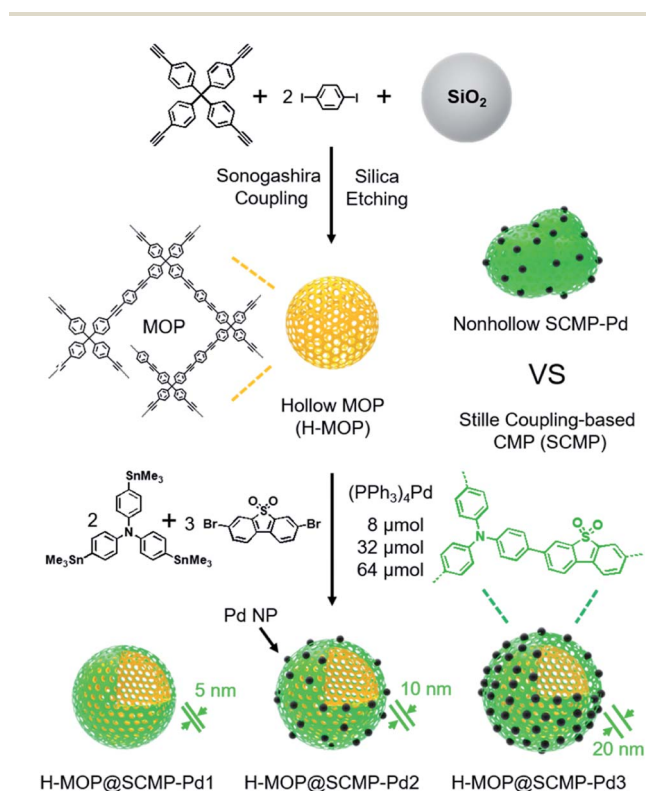


Fig. 1 Synthesis of H-MOP@SCMP-Pds and nonhollow SCMP-Pd.

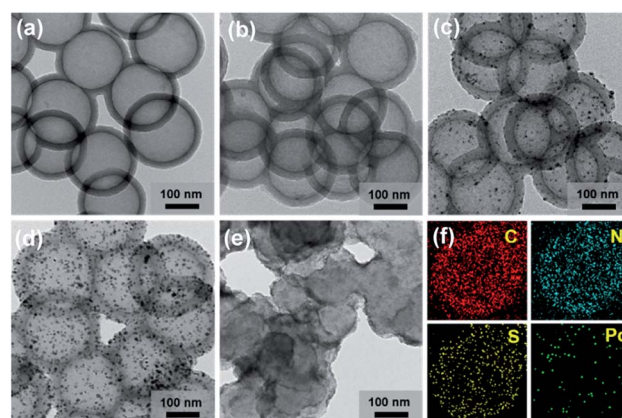


Fig. 2 TEM images of (a) H-MOP, (b) H-MOP@SCMP-Pd1, (c) H-MOP@SCMP-Pd2, (d) H-MOP@SCMP-Pd3, and (e) SCMP-Pd (also, refer to Fig. S11 in the ESI† for additional TEM and SEM images of H-MOP@SCMP-Pd2). (f) EDS elemental mapping images of H-MOP@SCMP-Pd2.

The surface areas (SAs) and microporosity of H-MOP, H-MOP@SCMP-Pds, and nonhollow SCMP-Pd were characterized by the analysis of N_2 adsorption-desorption isotherm curves based on the Brunauer–Emmett–Teller theory and the nonlocal density functional theory (NLDFT) method (Fig. 3a and b, S1, and Table S1 in the ESI†). Whilst the SA of H-MOP was measured to be $610 \text{ m}^2 \text{ g}^{-1}$, that of H-MOP@SCMP-Pd1 was reduced to $405 \text{ m}^2 \text{ g}^{-1}$, possibly due to the pore-clogging of inner H-MOP by the SCMP-Pd and the relatively incomplete networking of SCMP. The micropore volumes (V_{mic}) of H-MOP and H-MOP@SCMP-Pd1 were measured to be 0.14 and $0.10 \text{ cm}^3 \text{ g}^{-1}$, respectively. The SA and V_{mic} of H-MOP@SCMP-Pd2

increased to $507 \text{ m}^2 \text{ g}^{-1}$ and $0.11 \text{ cm}^3 \text{ g}^{-1}$, respectively, due to the increased amount of SCMP and the enhanced networking of SCMP by the increased $(\text{PPh}_3)_4\text{Pd}$ catalyst. In the case of H-MOP@SCMP-Pd3, the SA and V_{mic} decreased to $482 \text{ m}^2 \text{ g}^{-1}$ and $0.11 \text{ cm}^3 \text{ g}^{-1}$, due to the increased amount of Pd nanoparticles. Interestingly, nonhollow SCMP-Pd showed a poor SA of $115 \text{ m}^2 \text{ g}^{-1}$ with V_{mic} of $0.02 \text{ m}^2 \text{ g}^{-1}$, possibly due to the incomplete networking and the clogging of micropores by Pd nanoparticles.

The Pd species in the H-MOP, H-MOP@SCMP-Pds, and SCMP-Pd were investigated by powder X-ray diffraction (PXRD) studies and X-ray photoelectron spectroscopy (XPS) (Fig. 3c and S2 in the ESI†). Whilst the PXRD patterns of H-MOP and H-MOP@SCMP-Pd1 were amorphous, due to the minor amount of Pd, that of H-MOP@SCMP-Pd2 showed a broad diffraction peak at 2θ of 39.4° , corresponding to the (111) crystalline plane of metallic Pd (JCPDS# 05-0681) (Fig. 3c).³¹ In the PXRD pattern of H-MOP@SCMP-Pd3, the intensities of Pd diffraction peaks increased at 2θ of 39.4° , 45.9° , and 67.2° , corresponding to the (111), (200), and (220) crystalline planes of metallic Pd, respectively. In comparison, the nonhollow SCMP-Pd showed a very broad Pd diffraction peak at 2θ of $\sim 39.5^\circ$, due to the relatively smaller sizes of Pd particles.

In the XPS spectrum of H-MOP, the 3d orbital peaks of Pd(2+) state appeared at 337.0 and 342.4 eV (Fig. S2 in the ESI†).³² Whilst the Pd 3d orbital peaks were not distinguishable in the XPS spectrum of H-MOP@SCMP-Pd1, those of H-MOP@SCMP-Pd2, H-MOP@SCMP-Pd3, and SCMP-Pd showed the 3d orbital peaks of zerovalent Pd state at 336.1 and 341.4 eV.³³ According to the inductively coupled plasma (ICP) analysis, the contents of Pd in H-MOP, H-MOP@SCMP-Pd1, H-MOP@SCMP-Pd2, H-MOP@SCMP-Pd3, and SCMP-Pd were analyzed to be 0.92, 1.2, 6.4, 11, and 5.8 wt%, respectively. The combustion elemental analysis indicated that the contents of triphenylamines in the H-MOP@SCMP-Pd1, H-MOP@SCMP-Pd2, H-MOP@SCMP-Pd3, and SCMP-Pd are 1.54, 1.24, 0.95, and 1.23 mmol g^{-1} , respectively. In addition, the contents of dibenzothiophene sulfone moieties in H-MOP@SCMP-Pd1, H-MOP@SCMP-Pd2, H-MOP@SCMP-Pd3, and SCMP-Pd were analyzed to be 1.28, 1.11, 0.81, and 1.33 mmol g^{-1} , respectively. The comparable contents of triphenylamines and dibenzothiophene sulfones in the H-MOP@SCMP-Pd2 and SCMP-Pd indicate the relatively incomplete networking and the significant existence of coupling groups in nonhollow SCMP-Pd.

The chemical structures of H-MOP, H-MOP@SCMP-Pds, and SCMP-Pd were further characterized by infrared absorption (IR) and solid state ^{13}C nuclear magnetic resonance (NMR) spectroscopy (Fig. 3d and e). In the IR spectra, aromatic C=C and C-H vibration peaks of H-MOP and H-MOP@SCMP-Pds appeared at 1503 and 826 cm^{-1} , respectively³⁴ (Fig. 3d). As the amount of SCMP increased, the intensities of new aromatic C=C vibration peaks increased at 1465 and 1597 cm^{-1} with decrease of the vibration peak of H-MOP at 1503 cm^{-1} . In addition, new vibration peaks appeared at 1161 and 1307 cm^{-1} in the IR spectra of H-MOP@SCMP-Pds, corresponding to the O=S=O group of the dibenzothiophene sulfone moieties.³⁵

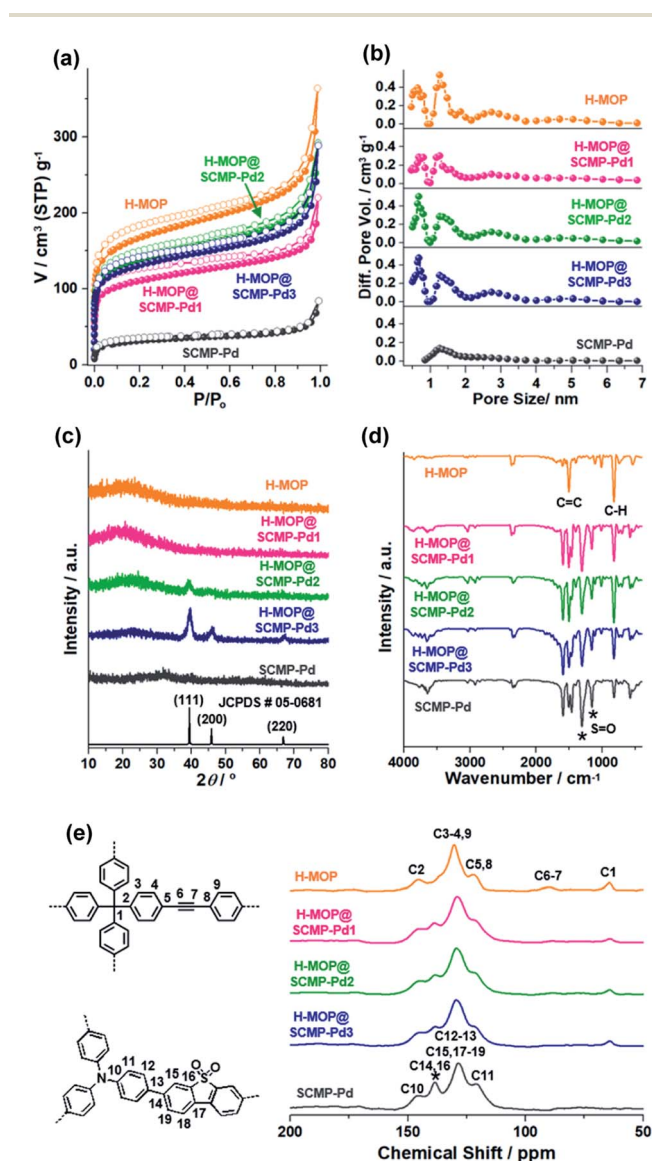


Fig. 3 (a) N_2 sorption isotherm curves obtained at 77 K, (b) pore size distribution diagrams based on the NLDFT method, (c) PXRD patterns, (d) IR spectra, and (e) solid state ^{13}C NMR spectra of H-MOP and H-MOP@SCMP-Pds, and SCMP-Pd. The asterisks of the IR spectrum of SCMP-Pd correspond to the S=O vibrations and that of ^{13}C NMR spectrum corresponds to the adjacent carbons to S in dibenzothiophene sulfone moieties.

The ^{13}C NMR spectrum of H-MOP showed aromatic ^{13}C peaks at 122, 130, 136, and 146 ppm (Fig. 3e). In addition, the ^{13}C peaks of the internal alkyne and benzyl carbon appeared at 90 and 64 ppm, respectively, matching well with those reported in the literature.³⁴ As the amount of SCMP in H-MOP@SCMP-Pds increased, the intensities of internal alkyne ^{13}C peaks at 90 ppm decreased gradually. In addition, the aromatic ^{13}C peaks of H-MOP@SCMP-Pds changed significantly, compared with those of H-MOP. Especially, new peaks appeared at 138 ppm, corresponding to the adjacent carbons to S in dibenzothiophene sulfone moieties. The ^{13}C NMR and IR spectra indicate that the SCMP was successfully incorporated in H-MOP@SCMP-Pds.

The optical properties of H-MOP, H-MOP@SCMP-Pds, and SCMP-Pd were investigated by the reflectance and emission spectroscopy (Fig. 4). As the amounts of Pd nanoparticles in the H-MOP@SCMP-Pds and SCMP-Pd increased, their colors changed gradually from greenish yellow to dark green (Fig. 4a–e). Compared with H-MOP, the H-MOP@SCMP-Pds and SCMP-Pd showed new absorption bands at 375–500 nm, corresponding to the feature of SCMP (Fig. 4f). In addition, H-MOP@SCMP-Pd2, H-MOP@SCMP-Pd3, and SCMP-Pd showed broad absorption over 500–800 nm, due to the Pd nanoparticles. As the amount of Pd in the H-MOP@SCMP-Pds increased, the absorbance at 375–500 nm decreased with the increase of absorbance at 500–800 nm (Fig. 4f). In emission spectra, whilst the H-MOP was not emissive, the H-MOP@SCMP-Pds and SCMP-Pd showed emission at 546–548 nm (Fig. 4g). As the amounts of Pd species increased, the emission intensities at 546–548 nm decreased in the order of H-MOP@SCMP-Pd1 (1) > SCMP-Pd (0.63) > H-MOP@SCMP-Pd2 (0.37) > H-MOP@SCMP-Pd3 (0.31). The emission quantum yields of H-MOP@SCMP-Pd1, SCMP-Pd, H-MOP@SCMP-Pd2, and H-MOP@SCMP-Pd3 were measured to

be 3.1, 2.8, 1.8, and 0.9%, respectively.³⁶ The average emission life times (τ_{avg}) of H-MOP@SCMP-Pd1, SCMP-Pd, H-MOP@SCMP-Pd2, and H-MOP@SCMP-Pd3 were measured to be 9.4, 8.6, 7.3, and 7.0 ns, respectively (Fig. S3 in the ESI†). In a mixture of water and 10% triethanolamine (TEOA), the τ_{avg} values of H-MOP@SCMP-Pd1, SCMP-Pd, H-MOP@SCMP-Pd2, and H-MOP@SCMP-Pd3 decreased to 2.9, 2.5, 2.3, and 2.0 ns, respectively. The emission quenching of H-MOP@SCMP-Pds and SCMP-Pd by Pd nanoparticles and a mixture of water and TEOA indicates the photo-induced electron transfer from SCMP to Pd nanoparticles and an aqueous medium.

Considering the photophysical properties and good dispersity in water (Fig. S4 in the ESI†), we studied the catalytic performance of H-MOP@SCMP-Pds (0.13 mg mL⁻¹) for the visible light (a 300 W Xe lamp, <400 nm cut off, 530 mW cm⁻²)-induced hydrogen evolution (Fig. 5a and b and refer to the ESI† for details).

Whilst the control material, H-MOP showed a nearly no HER, H-MOP@SCMP-Pd1 showed a HER of 1400 $\mu\text{mol h}^{-1} \text{g}^{-1}$ for 5 h (Fig. 5a). In the case of H-MOP@SCMP-Pd2, a HER dramatically increased to 7100 $\mu\text{mol h}^{-1} \text{g}^{-1}$ (14 $\mu\text{mol h}^{-1} \text{m}^{-2}$), due to the existence of Pd nanoparticles and enhanced porosity. At the 1 sun light intensity, the HER of the H-MOP@SCMP-Pd2 was measured to be 5700 $\mu\text{mol h}^{-1} \text{g}^{-1}$ (Fig. S5 in the ESI†). In the photocatalytic system of H-MOP@SCMP-Pd3, a HER was reduced to 4800 $\mu\text{mol h}^{-1} \text{g}^{-1}$, due to the reduced visible light absorption at 400–500 nm. Thus, among H-MOP@SCMP-Pds, the H-MOP@SCMP-Pd2 with TEOA as an electron sacrifier was identified as an optimized system (Fig. S5 in the ESI†). In the control tests, the H-MOP@SCMP that was prepared by the Pd etching of H-MOP@SCMP-Pd2 showed very poor HER performance, indicating the catalytic role of Pd nanoparticles (Fig. S5 in the ESI†). In comparison, the nonhollow SCMP-Pd showed a HER of 3200 $\mu\text{mol h}^{-1} \text{g}^{-1}$, due to the elongated diffusion pathway of the electron sacrifier into the materials. The H₂ evolution by H-MOP@SCMP-Pd2 was saturated at the concentration of 2.5 mg mL⁻¹, due to the inefficient light absorption by self-blocking effect (Fig. S6 in the ESI†). The HER performance of H-MOP@SCMP-Pd2 is superior or comparable to the recent CMP-based photocatalysts with Pd species (Table S2 in the ESI† and also, refer to a recent review paper²).^{1–12,28–30,37–43} The excellent HER performance of H-MOP@SCMP-Pd2 is attributable to the hollow morphology effect (the generation of more catalysts using the same amount of materials),¹⁸ the harmonized amount of SCMP and Pd nanoparticles, the high surface area, and thin shell-induced short diffusion pathways^{19,20} of redox substrates. While the H-MOP platform induced the hollow morphology engineering of H-MOP@SCMP-Pd2, at the same time, it facilitated the networking process in the formation of SCMP materials (Table S1 in the ESI†). It is also noteworthy that the near IR absorption by metallic nanoparticles can contribute to the photocatalytic hydrogen evolution.^{44,45}

According to the computational simulation on model systems (refer to the ESI† for details), the HOMO and LUMO energy levels of SCMP were calculated to be -5.05 and -1.97 eV, respectively, indicating the facile photo-induced electron transfer to the protons (Fig. S7–S10 in the ESI†). The electron

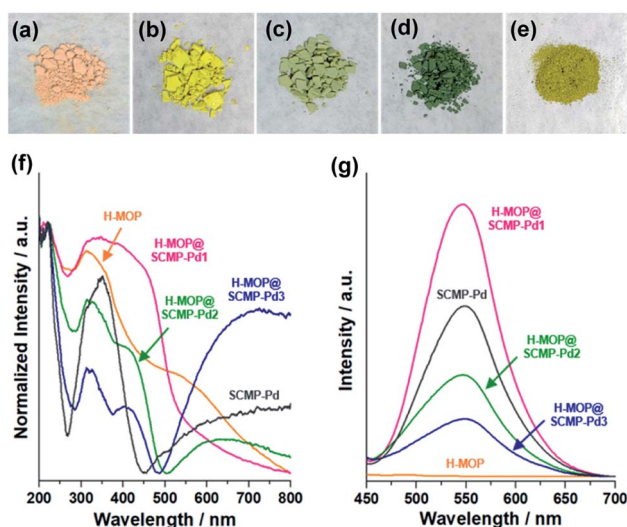


Fig. 4 Photographs of (a) H-MOP, (b) H-MOP@SCMP-Pd1, (c) H-MOP@SCMP-Pd2, (d) H-MOP@SCMP-Pd3, and (e) SCMP-Pd. (f) UV/vis absorption (powder) and (g) emission spectra (aqueous suspensions, 0.13 mg mL⁻¹, λ_{ex} = 420 nm) of H-MOP, H-MOP@SCMP-Pds, and SCMP-Pd.

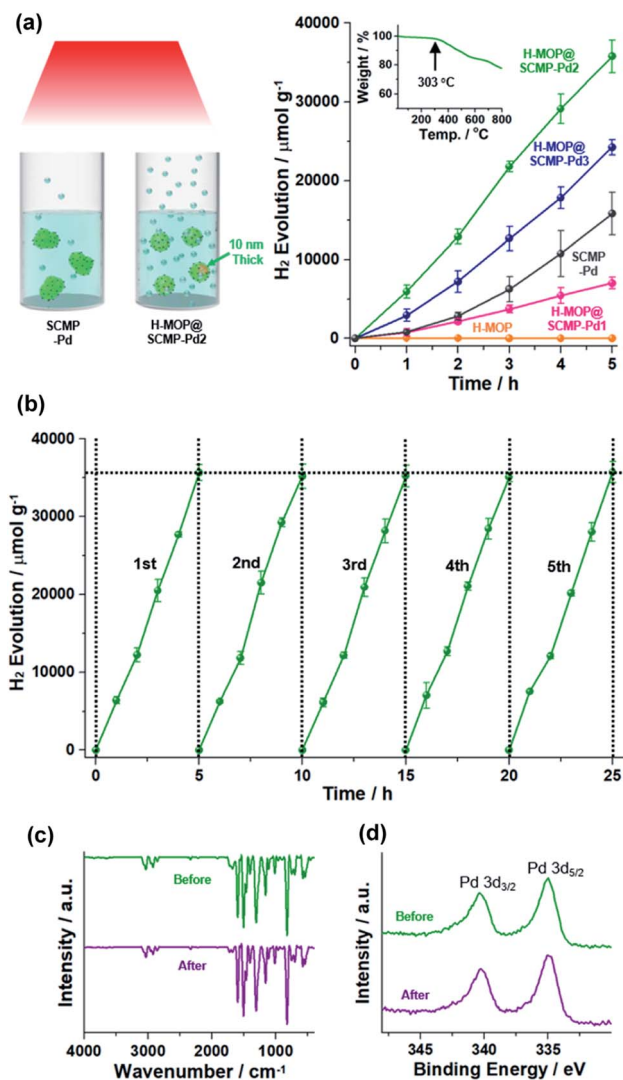


Fig. 5 (a) Hydrogen evolution performance (average values of five sets) of H-MOP, H-MOP@SCMP-Pds, and SCMP-Pd (a 300 W Xe lamp with an <400 nm optical filter and light intensity of 530 mW cm^{-2} , 10 v/v% TEOA as an electron sacrifier, 0.13 mg mL^{-1} photocatalyst, $21 \pm 1 \text{ }^\circ\text{C}$), a TGA curve of H-MOP@SCMP-Pd2 (inset), and (b) recyclability tests of hydrogen evolution by H-MOP@SCMP-Pd2 (hydrogen was evacuated after every 5 h). (c) IR and (d) XPS spectra of H-MOP@SCMP-Pd2 before and after five successive reactions.

densities of the simulated HOMO and LUMO of SCMP were mainly distributed at triphenylamine and dibenzothiophene sulfone moieties, respectively, indicating that the photo-induced charge transfer occurs from the electron-rich triphenylamines to the electron-deficient dibenzothiophene sulfone moieties (Fig. S8 in the ESI†).

The thermogravimetric analysis (TGA) indicated that the H-MOP@SCMP-Pd2 was stable up to $303 \text{ }^\circ\text{C}$ (inset of Fig. 5a). Considering the stability, we conducted the recyclability tests, showing that the H-MOP@SCMP-Pd2 maintained HERs in the range of $7000\text{--}7100 \text{ } \mu\text{mol h}^{-1} \text{ g}^{-1}$ in the five successive cycles (Fig. 5b). The microscopic studies, IR, and XPS analysis of the H-MOP@SCMP-Pd2 recovered after 5 recycle reactions showed the

complete retention of the original morphologies and chemical structures (Fig. 5c and d and S11 in the ESI†).

The apparent quantum yield (AQY), a percent of the number of reacted electrons per the number of incident photons, is a valuable parameter for the further understanding of photocatalytic systems.^{46–48} The AQYs of H-MOP@SCMP-Pd2 were measured by using monochromatic light sources with wavelengths of 400, 420, and 500 nm (Fig. 6). The light intensities were measured to be 5.9 , 5.9 , and 10.7 mW cm^{-2} at the wavelengths of 400, 420, and 500 nm, respectively. As the concentrations of H-MOP@SCMP-Pd2 increased from 0.13 mg mL^{-1} to 0.63 , 1.3 and 2.5 mg mL^{-1} , the absolute amount of the generated H_2 increased with an increase of the AQYs (@420 nm) from 0.89% to 1.76 , 3.34 , and 3.72% , respectively (Fig. S12 in the ESI†). The best 3.72% AQY (@420 nm) of H-MOP@SCMP-Pd2 is comparable or superior to those in the literature (Table S2 in the ESI†).^{3,11,13,39,43} Whilst H-MOP@SCMP-Pd2 (2.5 mg mL^{-1}) showed a significant AQY of 2.56% at 400 nm , the AQY sharply dropped to 0.46% at 500 nm , matching with the absorption feature of H-MOP@SCMP-Pd2 (Fig. 4f and 6).

In conclusion, H-MOP@SCMP-Pds with a hollow structure and Pd nanoparticles were engineered by template synthesis. H-MOP could be used as a template in the hollow shape engineering of the SCMP. At the same time, the concomitant formation of Pd nanoparticles could be induced in the synthesis of SCMP. The resultant H-MOP@SCMP-Pds showed promising HER activities up to $7100 \text{ } \mu\text{mol h}^{-1} \text{ g}^{-1}$ and AQYs up to 3.72% . The HER activities of H-MOP@SCMP-Pds were dependent on the harmonized amount of SCMP and Pd nanoparticles. The optimized H-MOP@SCMP-Pd2 maintained the HER activities in the range of $7000\text{--}7100 \text{ } \mu\text{mol h}^{-1} \text{ g}^{-1}$ in the five successive cycles. The enhanced HER performance of H-MOP@SCMP-Pd2 is attributable to the hollow structure, efficient visible light absorption, and the catalytic role of Pd nanoparticles. Based on the shape engineering methodology presented in this work, we believe that more various CMP-based photocatalysts can be engineered for hydrogen evolution from aqueous media and overall water splitting.^{43,49–51}

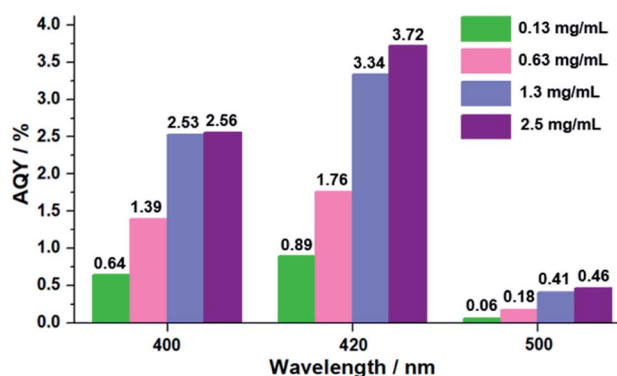


Fig. 6 Apparent quantum yields of H-MOP@SCMP-Pd2 (light intensities of 5.9 , 5.9 , and 10.7 mW cm^{-2} at 400, 420, and 500 nm, respectively, 10 v/v% TEOA as an electron sacrifier, $21 \pm 1 \text{ }^\circ\text{C}$).

Author contributions

S. U. Son: conceptualization, supervision, writing original draft, and review & editing. K. C. Ko: investigation, formal analysis, writing original draft, and review & editing. S. H. Ryu, S. M. Lee, and Y.-J. Ko: investigation and formal analysis. H. J. Kim: formal analysis and supervision.

Conflicts of interest

There are no conflicts to declare.

Acknowledgements

This work was supported by the National Research Foundation of Korea (NRF) grant (no. 2020R1A2C200431011) and Basic Science Research program (NRF-2020R1F1A1076128) funded by the Korea government (MSIT).

Notes and references

- J. H. Park, K. C. Ko, N. Park, H.-W. Shin, E. Kim, N. Kang, J. H. Ko, S. M. Lee, H. J. Kim, T. K. Ahn, J. Y. Lee and S. U. Son, *J. Mater. Chem. A*, 2014, **2**, 7656–7661.
- Y. Wang, A. Vogel, M. Sachs, R. S. Sprick, L. Wilbraham, S. J. A. Moniz, R. Godin, M. A. Zwijnenburg, J. R. Durrant, A. I. Cooper and J. Tang, *Nat. Energy*, 2019, **4**, 746–760.
- R. S. Sprick, J.-X. Jiang, B. Bonillo, S. Ren, T. Ratvijitvech, P. Guignon, M. A. Zwijnenburg, D. J. Adams and A. I. Cooper, *J. Am. Chem. Soc.*, 2015, **137**, 3265–3270.
- Y. Bai, L. Wilbraham, B. S. Slater, M. A. Zwijnenburg, R. S. Sprick and A. I. Cooper, *J. Am. Chem. Soc.*, 2019, **141**, 9063–9071.
- L. Li, W.-Y. Lo, Z. Cai, N. Zhang and L. Yu, *Macromolecules*, 2016, **49**, 6903–6909.
- Y. S. Kochergin, D. Schwarz, A. Acharjya, A. Ichangi, R. Kulkarni, P. Eliášová, J. Vacek, J. Schmidt, A. Thomas and M. J. Bojdys, *Angew. Chem., Int. Ed.*, 2018, **57**, 14188–14192.
- X.-J. Xiao, Y. Wang, W.-R. Wang, J. Li, J. Wang, Z.-W. Xu, J. Li, J. Yao and W.-S. Li, *Macromolecules*, 2020, **53**, 2454–5463.
- H. Yang, H. Amari, L. Liu, C. Zhao, H. Gao, A. He, N. D. Browning, M. A. Little, R. S. Sprick and A. I. Cooper, *Nanoscale*, 2020, **12**, 24488–24494.
- Y. Xiang, X. Wang, L. Rao, P. Wang, D. Huang, X. Ding, X. Zhang, S. Wang, H. Chen and Y. Zhu, *ACS Energy Lett.*, 2018, **3**, 2544–2549.
- C. Yang, B. C. Ma, L. Zhang, S. Lin, S. Ghasimi, K. Landfester, K. A. I. Zhang and X. Wang, *Angew. Chem., Int. Ed.*, 2016, **55**, 9202–9206.
- R. S. Sprick, Y. Bai, A. A. Y. Guibert, M. Zbiri, C. M. Aitchison, L. Wilbraham, Y. Yan, D. J. Woods, M. A. Zwijnenburg and A. I. Cooper, *Chem. Mater.*, 2019, **31**, 305–313.
- C. Wang, H. Fan, X. Ren, Y. Wen and W. Wang, *Appl. Surf. Sci.*, 2018, **462**, 423–432.
- L. Li, Z. Cai, Q. Wu, W.-Y. Lo, N. Zhang, L. X. Chen and L. Yu, *J. Am. Chem. Soc.*, 2016, **138**, 7681–7686.
- M. Sachs, H. Cha, J. Kosco, C. M. Aitchison, L. Francàs, S. Coby, C.-L. Chiang, A. A. Wilson, R. Godin, A. Fahey-Williams, A. I. Cooper, R. S. Sprick, I. McCulloch and J. R. Durrant, *J. Am. Chem. Soc.*, 2020, **142**, 14574–14587.
- K. L. Skubi, T. R. Blum and T. P. Yoon, *Chem. Rev.*, 2016, **116**, 10035–10074.
- D. L. Ashford, A. M. Lapides, A. K. Vannucci, K. Hanson, D. A. Torelli, D. P. Harrison, J. L. Templeton and T. J. Meyer, *J. Am. Chem. Soc.*, 2014, **136**, 6578–6581.
- S. H. Ryu, S. J. Choi, J. H. Seon, B. Jo, S. M. Lee, H. J. Kim, Y.-J. Ko, K. C. Ko, T. K. Ahn and S. U. Son, *Catal. Sci. Technol.*, 2020, **10**, 5535–5543.
- G. Prieto, H. Tüysüz, N. Duyckaerts, J. Knossalla, G.-H. Wang and F. Schüth, *Chem. Rev.*, 2016, **116**, 14056–14119.
- K. Cho, J. Yoo, H.-W. Noh, S. M. Lee, H. J. Kim, Y.-J. Ko, H.-Y. Jang and S. U. Son, *J. Mater. Chem. A*, 2017, **5**, 8922–8926.
- J. H. Ko, N. Kang, N. Park, H.-W. Shin, S. Kang, S. M. Lee, H. J. Kim, T. K. Ahn and S. U. Son, *ACS Macro Lett.*, 2015, **4**, 669–672.
- L. Ma, H. Fan, K. Fu, S. Lei, Q. Hu, H. Huang and G. He, *ACS Sustainable Chem. Eng.*, 2017, **5**, 7093–7103.
- X. Ren, H. Fan, J. Ma, C. Wang, M. Zhang and N. Zhao, *Appl. Surf. Sci.*, 2018, **441**, 194–203.
- N. Kang, J. H. Park, M. Jin, N. Park, S. M. Lee, H. J. Kim, J. M. Kim and S. U. Son, *J. Am. Chem. Soc.*, 2013, **135**, 19115–19118.
- K. Zhang, D. Kopetzki, P. H. Seeberger, M. Antonietti and F. Vilela, *Angew. Chem., Int. Ed.*, 2013, **52**, 1432–1436.
- S. J. Choi, E. H. Choi, C. Song, Y.-J. Ko, S. M. Lee, H. J. Kim, H.-Y. Jang and S. U. Son, *ACS Macro Lett.*, 2019, **8**, 687–693.
- S. H. Ryu, D. H. Lee, S. M. Lee, H. J. Kim, Y.-J. Ko, K. C. Ko and S. U. Son, *Chem. Commun.*, 2019, **55**, 9515–9518.
- S. Yuan, S. Kirklin, B. Dorney, D.-J. Liu and L. Yu, *Macromolecules*, 2009, **42**, 1554–1559.
- Y. Zhao, W. Ma, Y. Xu, C. Zhang, Q. Wang, T. Yang, X. Gao, F. Wang, C. Yan and J.-X. Jiang, *Macromolecules*, 2018, **51**, 9502–9508.
- Z. Wang, X. Yang, T. Yang, Y. Zhao, F. Wang, Y. Chen, J. H. Zeng, C. Yan, F. Huang and J.-X. Jiang, *ACS Catal.*, 2018, **8**, 8590–8596.
- X. Gao, C. Shu, C. Zhang, W. Ma, S.-B. Ren, F. Wang, Y. Chen, J. H. Zeng and J.-X. Jiang, *J. Mater. Chem. A*, 2020, **8**, 2404–2411.
- Y. Xiong, J. M. McLellan, Y. Yin and Y. Xia, *Angew. Chem., Int. Ed.*, 2007, **46**, 790–794.
- G. B. Hoflund, H. A. E. Hagelin, J. F. Weaver and G. N. Salaita, *Appl. Surf. Sci.*, 2003, **205**, 102–112.
- Y. Holade, C. Canaff, S. Poulin, T. W. Napporn, K. Servat and K. B. Kokoh, *RSC Adv.*, 2016, **6**, 12627–12637.
- C. W. Kang, S. M. Lee, H. J. Kim, Y.-J. Ko and S. U. Son, *ACS Sustainable Chem. Eng.*, 2020, **8**, 13900–13907.
- Q. Zhou, S. Fu, M. Zou, Y. He, Y. Wu and T. Wu, *RSC Adv.*, 2015, **5**, 69388–69393.
- K. Suzuki, A. Kobayashi, S. Kaneko, K. Takehira, T. Yoshihara, H. Ishida, Y. Shiina, S. Oishi and S. Tobita, *Phys. Chem. Chem. Phys.*, 2009, **11**, 9850–9860.

- 37 M. G. Schwab, M. Hamburger, X. Feng, J. Shu, H. W. Spiess, X. Wang, M. Antonietti and K. Müllen, *Chem. Commun.*, 2010, **46**, 8932–8934.
- 38 L. Li and Z. Cai, *Polym. Chem.*, 2016, **7**, 4937–4943.
- 39 R. S. Sprick, B. Bonillo, M. Sachs, R. Clowes, J. R. Durrant, D. J. Adams and A. I. Cooper, *Chem. Commun.*, 2016, **52**, 10008–10011.
- 40 L. Wang, Y. Wan, Y. Ding, S. Wu, Y. Zhang, X. Zhang, G. Zhang, Y. Xiong, X. Wu, J. Yang and H. Xu, *Adv. Mater.*, 2017, **29**, 1702428.
- 41 Y. Xu, N. Mao, S. Feng, C. Zhang, F. Wang, Y. Chen, J. Zeng and J.-X. Jiang, *Macromol. Chem. Phys.*, 2017, **218**, 1700049.
- 42 Y. Xu, C. Zhang, P. Mu, N. Mao, X. Wang, Q. He, F. Wang and J.-X. Jiang, *Sci. China: Chem.*, 2017, **60**, 1075–1083.
- 43 L. Wang, X. Zheng, L. Chen, Y. Xiong and H. Xu, *Angew. Chem., Int. Ed.*, 2018, **57**, 3454–3458.
- 44 N. Ortiz, B. Zeollner, S. J. Hong, Y. Ji, T. Wang, Y. Liu, P. A. Maggard and G. Wang, *ACS Appl. Mater. Interfaces*, 2017, **9**, 25962–25969.
- 45 K. K. Patra and C. S. Gopinath, *J. Phys. Chem. C*, 2018, **122**, 1206–1214.
- 46 M. Melchionna and P. Fornasiero, *ACS Catal.*, 2020, **10**, 5493–5501.
- 47 M. Qureshi and K. Takanebe, *Chem. Mater.*, 2017, **29**, 158–167.
- 48 S. Cao and L. Piao, *Angew. Chem.*, 2020, **132**, 18468–18476.
- 49 G. Zhang, Z.-A. Lan, L. Lin, S. Lin and X. Wang, *Chem. Sci.*, 2016, **7**, 3062–30666.
- 50 S. Zhang, G. Cheng, L. Guo, N. Wang, B. Tan and S. Jin, *Angew. Chem., Int. Ed.*, 2019, **59**, 6007–6014.
- 51 Y. Bai, K. Nakagawa, A. J. Cowan, C. M. Aitchison, Y. Yamaguchi, M. A. Zwijnenburg, A. Kudo, R. S. Sprick and A. I. Cooper, *J. Mater. Chem. A*, 2020, **8**, 16283–16290.